THE JOURNAL OF PHYSICAL CHEMISTRY C

Article

pubs.acs.org/JPCC

Theoretical Study on the Diffusion Mechanism of Cd in the Cu-Poor Phase of $CuInSe_2$ Solar Cell Material

Janos Kiss,*[,†,‡] Thomas Gruhn,[†,§] Guido Roma,[†,∥] and Claudia Felser[†,‡]

[†]Johannes Gutenberg-Universität Mainz, Institut für Anorganische Chemie und Analytische Chemie, D-55128 Mainz, Germany

[‡]Max-Planck-Institut für Chemische Physik fester Stoffe, D-01187 Dresden, Germany

[§]Lehrstuhl für Material- und Prozesssimulation Universität Bayreuth, D-95447 Bayreuth, Germany

[∥]CEA, DEN, Service de Recherches de Métallurgie Physique, F-91191 Gif sur Yvette, France

ABSTRACT: We have employed first-principles static and molecular dynamics (MD) calculations with semilocal and screened-exchange hybrid density functionals to study the diffusion of Cd in bulk $CuIn_5Se_8$, a copper-poor ordered vacancy compound of $CuInSe_2$. The diffusion mechanism and the underlying kinetics/energetics were investigated by combining ab initio metadynamics simulations and nudged elastic band (NEB) calculations. We found that the migration of Cd occurs via a kick-out of Cu atoms, assisted by the pristine vacancies that are constitutive of this compound, and follows a double-hump energy profile. The rate-limiting step has a barrier of about 1 eV at 0 K but reduces to 0.3 eV at 850 K, pointing out non-negligible dynamical effects. Hybrid functional calculations reveal that Cd impurities are doubly positively charged (Cd^{2+}) in *p*-type and intrinsic conditions. The position of the 0/2+ charge transition level explains why Cd impurities do not constitute deep traps for carriers, making them not harmful for the solar cell device.

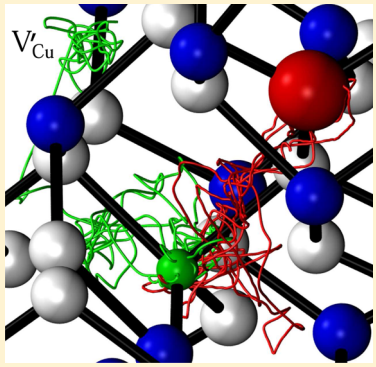

INTRODUCTION

Thin-film solar cells based on $CuInSe_2$ (CIS) or $Cu(In,Ga)Se_2$ (CIGS) materials have a recognized position in the solar cell market thanks to their outstanding price/performance ratio.[1] Because of their use in large-scale industrial deployments as well as for household installations, improvements in efficiency are actively sought, especially by trying to reduce losses at the interfaces of these complex multilayer devices.

In the standard manufacturing processes, after the growth of the light absorber, taking place at 550−650 °C,[2] a CdS buffer layer is added by chemical bath deposition at 60−80 °C.[3,4] Annealing at higher temperatures (200 °C) has sometimes been used to enhance the device efficiency.[5] Via different experimental techniques, it was shown that at the interface with CdS the CIS/CIGS absorber is strongly Cu depleted.[6,7] In the literature, these Cu-poor phases are widely accepted to be ordered vacancy compounds (OVCs) of $CuInSe_2$.[8−11]

Theoretically, the interplay of Cu depletion and Cd incorporation has been investigated very recently, showing that a relatively large amount of Cd, on the order of 1%, can indeed be present in the Cu-poor phase even at low temperatures.[12] Upon elevated deposition temperatures the Cd dopant atoms are prone to diffuse into the underlying Cu-poor absorber material.[13] Although such diffusion processes are highly relevant, and steer the performance of solar cells, there is only sparse data available regarding the diffusion mechanism of dopants and impurities.[4,14−18]

In particular, there are indications that the mobility of Cd, which seems to diffuse in the bulk and not through grain boundaries, could be higher in Cu-poor regions, possibly due to vacancy-assisted mechanisms.[4] The ratio of Cd and Cu diffusivities in the absorber and in the buffer layer is particularly important, as it contributes in determining the final morphology of the interface, probably through the Kirkendall effect.[19] Understanding the Cd diffusion mechanism and finding the optimal choice of the temperature treatments is of the utmost importance also for solar cells produced without a CdS buffer layer. For example, in cells produced by Cd implantation, the Cd diffusion is probably assisted by defects created by the implantation process and determines the final width of the inverted *n*-type layer.[17]

This has motivated us to investigate the diffusion of Cd impurities in Cu-poor CIS via theoretical calculations to widen our understanding on the diffusion process at the atomic scale, in particular in the Cu-poor region close to the interface with the buffer layer. Here we present a comprehensive large-scale ab initio study on the dynamics of Cd migration in bulk $CuIn_5Se_8$ based on Car−Parrinello dynamics[20] aided by metadynamics.[21] In addition, we also performed nudged elastic band (NEB) calculations, using both standard gradient-corrected density functional (PBE) and screened-exchange hybrid functional (HSE06) approaches.

RESULTS AND DISCUSSION

Computational Methodology. $CuIn_5Se_8$ is an ordered vacancy compound, obtained from $CuInSe_2$ by inserting a

Received: September 2, 2013
Revised: November 15, 2013
Published: November 19, 2013

   dx.doi.org/10.1021/jp4087877 | *J. Phys. Chem. C* 2013, 117, 25933−25938

periodic array of copper vacancies (V_{Cu}) and indium antisites (In_{Cu}) on Cu sublattice positions.[22−24] To distinguish them from other defect types, these constitutive defects are labeled in the following text by a prime (e.g., V'_{Cu}). In our calculations we have used the atomic configuration proposed by Zunger and co-workers for the chalcopyrite polytype of $CuIn_5Se_8$.[25,26] The unit cell of this structure is shown in Figure 1. To represent the

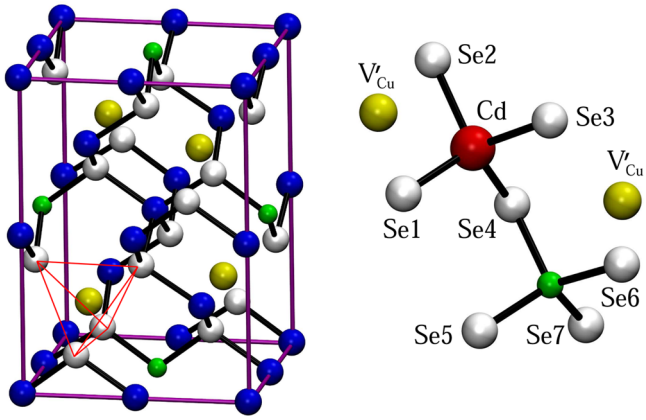

Figure 1. Left panel: conventional unit cell of the $CuIn_5Se_8$ ordered vacancy compound. A tetrahedron formed by four Se atoms surrounding a constitutive (or pristine) V'_{Cu} site is highlighted in red. The supercells used in our calculations contained eight conventional unit cells, having in total 224 atoms. Right panel: active reaction center and local surrounding of a Cd dopant atom sitting in a V'_{Cu} site. The Cu, In, Se, and Cd atoms are schematized as green, blue, gray, and red spheres, respectively, and the V'_{Cu} positions are shown in yellow.

bulk $CuIn_5Se_8$ we have employed a periodically repeated supercell model consisting of 2 × 2 × 2 tetragonal unit cells. The supercell had the dimensions of 16.53 Å × 16.53 Å × 23.47 Å and contained 224 atoms. The dynamical simulations were carried out using the CPMD[27] program package, a parallel implementation of density functional theory (DFT) based on plane waves, and pseudopotentials. We have employed the Perdew−Burke−Ernzerhof[28] (PBE) exchange-correlation functional and Vanderbilt-type ultrasoft pseudopotentials.[29] More details on the pseudopotentials used are available in our previous work.[12] The cutoff energies for the expansion of the valence wave function and the densities were set up to 25 and 100 Ry, respectively. Static calculations, with PBE and the HSE06[30,31] hybrid functional, were performed with the VASP code,[32] using the same supercells as for the dynamical simulations and Γ sampling of the Brillouin zone. For an improved description of the band gap of $CuIn_5Se_8$ we used a fraction of 0.30 of the exact exchange instead of the default HSE value of 0.25. For migration profiles a cutoff energy of 300 eV (22 Ry) proved sufficiently converged after various comparisons with results at 400 eV (29.4 Ry).

To study the diffusion of Cd atoms in bulk $CuIn_5Se_8$ we have performed ab initio molecular dynamics (MD) simulations based on the efficient Car−Parrinello MD scheme.[20] For the propagation of the system we have employed a fictitious electronic mass of 700 au and a time step of approximately 0.145 fs. The electronic and nuclear degrees of freedom were thermostatted using Nosé−Hoover chains.[33] As the starting structure we have used a fully optimized configuration, where a Cd atom was sitting in the center of mass of a tetrahedron formed by four 3-fold coordinated Se atoms (see Figure 1). This insertion site is preferred not only with respect to other substitutional sites[12] but most probably also with respect to other interstitial sites investigated for Cu in $CuInSe_2$,[34] where Cd, due to its larger size, is expected to have a formation energy equal to or higher than Cu. To achieve conditions relevant to the high-temperature production of solar cell materials in our simulation, we have slowly heated the system to 850 K with a temperature ramp of 170 K/ps. This was followed by an additional equilibration period of 3.5 ps.

In the time scale of first-principles MD simulations the structural or chemical transformations involving the breaking and formation of bonds are rare events. To accelerate the diffusion of Cd, we have used the metadynamics procedure, where Gaussian-shaped potential hills are added to the system to build up a history-dependent potential.[21] This potential discourages the nuclei to revisit points in the phase space. In our calculations each hill had a height of 0.019 eV. To prevent hill surfing a new hill was added only if the displacement of the collective coordinates was larger than 2/3 of the width of the biasing functions.[35] This method allowed us to map the free-energy surface involved in the chemical transformations along the diffusion path of Cd at a finite temperature and locate the lowest free-energy pathways between subsequent minima to calculate the free-energy barriers.[35] A similar methodology was used recently to investigate the dynamical processes on the polar and nonpolar surfaces of the CdTe solar cell material.[36]

Reaction Path from Metadynamics Simulations. To study the dynamical nature of the Cd diffusion, which cannot be captured by traditional static calculations, we have performed two distinct metadynamics simulations, characterized by different collective variables. To gain new insights about the diffusion path in the first scenario we have used a single collective variable: the distance between the Cartesian coordinates of the Cd atom and its original starting position. For this scenario we have obtained an accelerated diffusion path spanning 20 ps of ab initio metadynamics trajectory. We found that Cd explores with hardly any barrier the channels formed by the 3-fold coordinated Se atoms (shown with yellow spheres in Figure 1), without finding any further stable or metastable interstitial position, until it collides with one of the neighboring Cu atoms. The Cd atom is then repelled by Cu, and it drifts back toward its original starting position. During the simulation, after several of such collision events, the Cu was eventually kicked out into a neighboring V'_{Cu} site, leaving behind a V_{Cu} vacancy. Later the Cd atom squeezed into this newly created V_{Cu} vacancy site (see Figure 2). The calculated free-energy barrier for the kick-out of Cu via Cd was on the order of 0.3 eV. We remark that a similar mechanism involving Cu kick-out by indium atoms has been reported for $CuInSe_2$.[37] In that case, however, the efficiency of the mechanism to provide In self-diffusion is hindered by the limited availability of Cu vacancies, which are, conversely, naturally available in $CuIn_5Se_8$ as pristine vacancies.

For a more accurate description of the diffusion mechanism, in a subsequent simulation we have used three collective variables, which allowed us to analyze the individual processes in more detail. The three collective variables were the following: (I) the coordination number between Cd and the four Se atoms bound directly to Cd (see Se1, Se2, Se3, and Se4 from the right panel of Figure 1), (II) the coordination number between a Cu atom sitting in the first neighbor position to Cd and the four Se atoms directly bound to this specific Cu (see Se4, Se5, Se6, and Se7 from Figure 1), and (III) the

dx.doi.org/10.1021/jp4087877 | J. Phys. Chem. C 2013, 117, 25933−25938

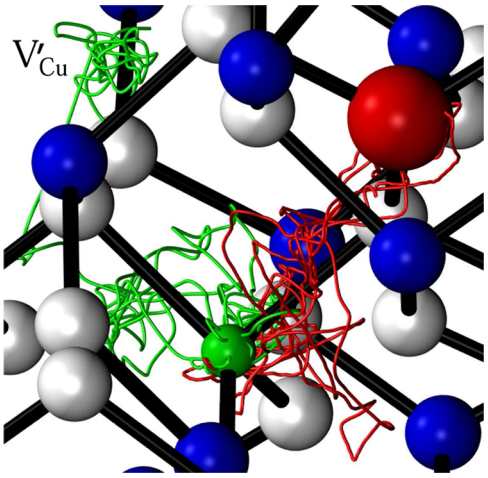

Figure 2. Inset from the 224 atom supercell showing the diffusion path of Cd and Cu atoms in $CuIn_5Se_8$ plotted along the metadynamics trajectory. The pathways sampled by Cd and Cu are traced with red and green splines, respectively. For the representation of the atoms the same color scheme as in Figure 1 was used.

coordination number of Cd relative to the four Se sitting in the first coordination sphere of the Cu atom described above (i.e., Se4, Se5, Se6, and Se7). In the following we will refer to these (I), (II), and (III) coordination numbers as c[Cd−Se−A], c[Cu−Se], and c[Cd−Se−B], respectively. The coordination numbers were defined based on ref 21 as

$$c[i] = \sum_{j \neq i}^{n} \frac{1 - \left(\frac{d_{ij}}{d_0}\right)^p}{1 - \left(\frac{d_{ij}}{d_0}\right)^{p+q}} \quad (1)$$

where the exponents are $p = 6$ and $p + q = 12$; the index j runs over the list of Se atoms described above; d_{ij} is the interatomic distance between atoms i and j; and d_0 is a reference cutoff distance. On the basis of the averaged Cd−Se and Cu−Se equilibrium distances of 2.71 and 2.48 Å measured during the equilibration procedure, the d_0 cutoff distances have been selected as 3.70, 3.40, and 3.70 Å for the coordination numbers I, II, and III, respectively. The chosen d_0 value assures that the contribution of atom j to the coordination number in equation 1—the bond switching function—does not fluctuate too much on the scale of phonon displacements but, at the same time, fluctuates enough even close to the equilibrium value to promote bond breaking. A sketch of the bond switching function including the position of the equilibrium bonding distances is shown in Figure 4. The evolution of the I, II, and III variables during the metadynamics simulation is shown in Figure 3.

Using this setup we have performed an extended ab initio metadynamics simulation spanning 45 ps of trajectory. We found that, first, the Cu was kicked out into an adjacent V'_{Cu} site by Cd (see green curve in Figure 3 and the path of Cu traced with green in Figure 2), leaving behind a V_{Cu} vacancy. Subsequently, Cd has migrated into the newly created V_{Cu} defect site and occupied it in the Cu sublattice (see red and blue curves in Figure 3 and the path of Cd traced with red in Figure 2). In both simulations we found that In and Se positions are not visited by Cd, indicating that Cd forms a defect complex with the surrounding pristine vacancies, and it prefers to sit in V_{Cu} positions of the Cu sublattice. Indeed, by

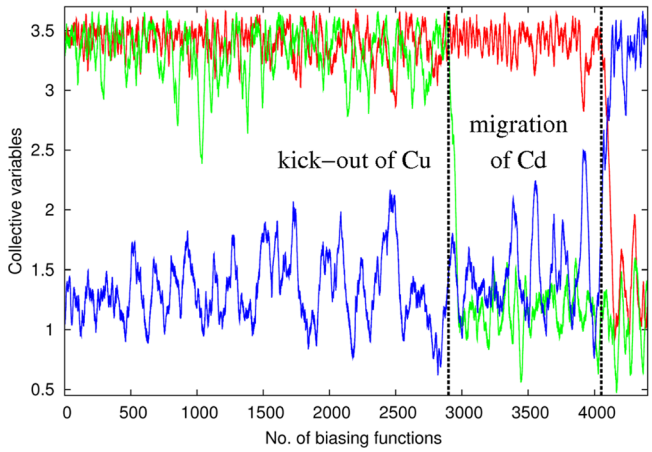

Figure 3. Dynamics of the collective variables as a function of the number of biasing potentials added to the system in the frame of 45 ps of accelerated ab initio metadynamics simulation. The three collective variables c[Cd−Se−A], c[Cu−Se], and c[Cd−Se−B] are shown in red, green, and blue color, respectively. The transitions from the reactant to the intermediate and from the intermediate to the final product state are indicated by vertical dashed lines.

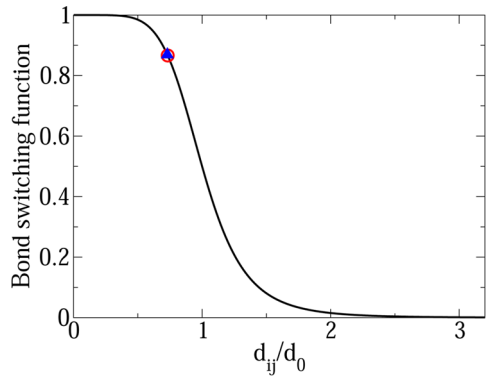

Figure 4. Shape of the bond switching function as a function of the ratio of the atomic distance versus the reference value, d_0. The circle and the triangle show the value of the bond switching function at the equilibrium bonding distance for Cd−Se and Cu−Se ($0.73 \times d_0$ in both cases).

computing the solution energies via static calculations in different sites of $CuIn_5Se_8$ the above-mentioned V_{Cu} positions were energetically the most favorable. These findings are in agreement with our previous work on neutral Cd stability,[12] according to which a further 0.2 eV can be gained by configurations where the displaced Cu atom is far from the Cd. Furthermore, the solution energy of Cd on In sites was 1.66 eV higher than on V_{Cu} sites, which clearly shows that the diffusion of Cd is most likely to take place along the Cu sublattice and the pristine V'_{Cu} sublattice.

On the basis of the reconstructed free-energy landscape (see Figure 5) our calculations reveal a double-hump energy profile, indicating that the most probable diffusion mechanism is a two-step process, leading from a starting configuration (reactant, shown in Figure 1) to an intermediate metastable state and eventually to a final state. The resulting free-energy barriers for the kick-out of Cu by Cd and for the subsequent migration of Cd were 0.31 and 0.23 eV, respectively, implying that the kick-out of Cu is the rate-limiting step.

dx.doi.org/10.1021/jp4087877 | J. Phys. Chem. C 2013, 117, 25933−25938

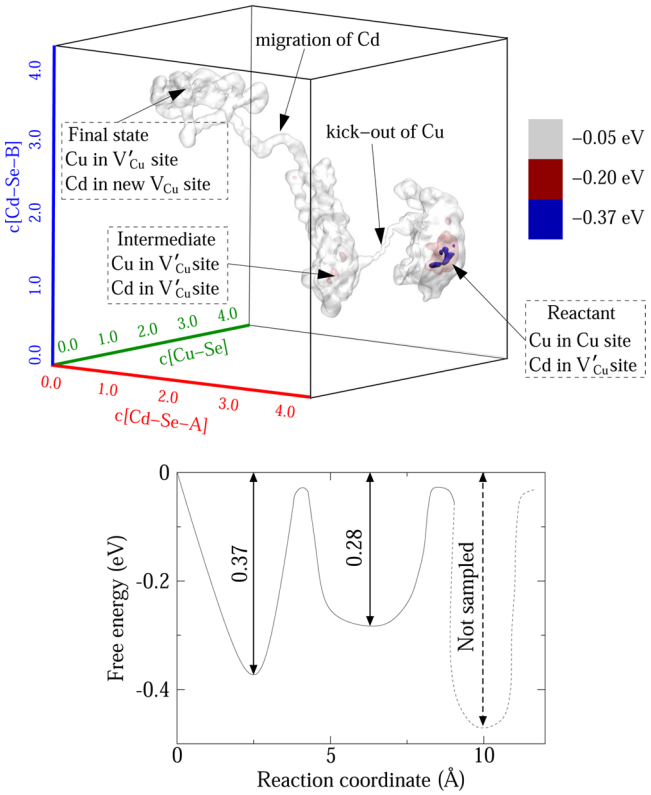

Figure 5. Top panel: Iso-surface representation of the reconstructed three-dimensional free-energy hypersurface of Cd diffusion. The third free-energy minimum corresponding to the final product state after the migration of Cd was just shortly visited and not fully explored. Bottom panel: Cartoon representation of the free-energy landscape, projected onto the NEB reaction coordinate (Cartesian distance) along the diffusion path.

Charge Transition Levels. The stable sites and trajectories found by metadynamics were then used in static NEB calculations, but before further discussing diffusion properties, we will comment on the energetics and on the charge transition levels. In our NEB calculations we have used both the PBE and HSE06 hybrid functional. The latter, with the modified fraction of exact exchange parameter, gives a band gap for $CuIn_5Se_8$ of 1.27 eV, in good agreement with experiment, which allowed us to study the charge stability of the Cd impurity. We performed the same calculations with PBE, for the sake of comparison, although semilocal functionals give a barely visible band gap for this compound (in our case 0.07 eV with PBE). Besides the band gap also the u free structural parameter is improved with the use of the HSE06 hybrid functional.[12]

The results of the HSE06 calculation for the neutral Cd impurity, for which two electrons occupy the conduction band, clearly suggest that the relevant charge state is $Q = 2+$. We nevertheless calculated NEB paths for both charge states to check possible charge effects along the migration path, and in the following we comment on the relative stability.

Solution energies for neutral Cd ($Q = 0$) and Cd^{2+} ($Q = 2+$) charge states are shown in Table 1, together with the $\varepsilon(0/2+)$ thermodynamic charge transition level, for the three minima along the migration path. We have not introduced electrostatic periodic image interaction corrections because the charge of the defect, whose energy levels are resonant with the band edges, is certainly delocalized. The Madelung monopole correction, even for our relatively large supercell, amounts to 0.4 eV, and the band alignment term (also not included in the values shown in Table 1) is on the order of 0.04 (0.05) eV for PBE (HSE06). We remark that PBE predicts that Cd impurities are almost always neutral for intrinsic, n-type and also for moderately p-type $CuIn_5Se_8$. Conversely, the HSE06 result, which is not flawed by the underestimation of the band gap, shows that Cd impurities in $CuIn_5Se_8$ are almost always charged 2+ because the charge transition level is situated less than 0.1 eV below the conduction band bottom. Although for such a shallow defect an accurate determination of the thermodynamic charge transition level would require even larger supercells, it is clear that, even in relatively strong n-type conditions, Cd impurities are positively charged and even more so if the Fermi level is around midgap, as recently measured for a similar CdS/Cu-poor CIS heterojunction.[11] This explains also why Cd impurities are not harmful for the device, as they do not act as deep interface traps for the minority carriers of the absorber (i.e., electrons).

Table 1. Solution Energies (in eV) of Cd Impurities in $CuIn_5Se_8$ with PBE and HSE06 for the Neutral and +2 Charge States (μ_e = VBT + 0.6, where VBT is the Valence Band Top), for the Three Configurations Corresponding to Minima along the Migration Path[a]

	PBE			HSE06		
configuration	0	2+	$\varepsilon(0/2+)$	0	2+	$\varepsilon(0/2+)$
reactant	−0.52	0.49	0.10	0.07	−1.19	1.23
intermediate	−0.26	0.77	0.09	0.34	−0.92	1.23
final state	−0.92	0.10	0.09	−0.40	−1.68	1.24

[a]The reference chemical potential for Cd is the bulk metallic phase. The corresponding $\varepsilon(0/2+)$ thermodynamic charge transition levels (referred to the VBT) are also shown.

Activation Energies from NEB Calculations. The metadynamics calculations presented above gave us, on the one hand, an estimation of free energy barriers at high temperature (850 K). The values show that by depositing CdS at the mild temperature of the chemical bath process one can avoid excessive Cd diffusion into the CIGS absorber, which would degrade material properties. On the other hand, the exploration of the energy landscape provided minimum energy paths which were investigated in more detail by static calculations. In addition to the free-energy barriers at 850 K we have then computed the activation energies at 0 K along the diffusion path via the climbing NEB method.[38] Static calculations allowed us to use hybrid functionals, which would have been prohibitive in a large-scale metadynamics calculation as the one previously presented. The results of the NEB calculations for the double-hump path are presented in Figure 6. Surprisingly, the effect of the inclusion of exact exchange on the migration barriers seems to be negligible, both qualitatively and even quantitatively. The analysis of energy contributions along the migration paths shows that the Fock-exchange term is almost constant during the jumps, and the essential part of the energy variations comes from the Hartree and Ewald electrostatic contributions, together with the one-electron band term; in the latter no contributions from defect levels in the band gap are present. This explains also the very weak influence of the charge state on migration barriers because the neutral state differs from the 2+ state only by the presence of two delocalized electrons in the conduction band, whose influence on the electrostatic energy is supposed to vary only weakly along the jump trajectory.

dx.doi.org/10.1021/jp4087877 | J. Phys. Chem. C 2013, 117, 25933−25938

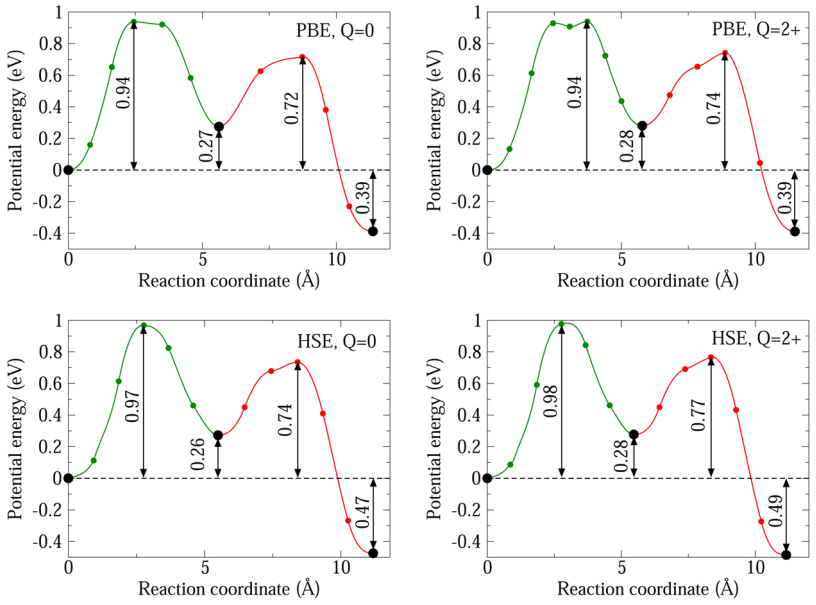

Figure 6. Comparison of minimum energy paths from NEB calculations, for the migration of Cd assisted by a kick-out of a copper atom. The reaction coordinate is the Cartesian distance in 3*N*-dimension (*N* = number of atoms in the supercell). The upper panels shows the results obtained with the standard PBE xc-functional. The lower panels feature the outcome of NEB calculations with the HSE06 hybrid functional. On the left the charge state is neutral ($Q = 0$), and on the right it is 2+ ($Q = 2+$). In all panels, the first barrier shown with green corresponds to the ejection of a Cu atom (by the neighboring Cd) from its lattice site. This Cu site, now left vacant, is then occupied by Cd after overcoming the second energy barrier (shown with red). The relative energies of the reactant, intermediate, and final product states are shown with large black dots.

The resulting activation energies are 0.97 (0.94) eV and 0.48 (0.45) eV with HSE06 (PBE), respectively, which are two to three times larger than the corresponding free-energy barriers at 850 K. This implies either a relatively large migration entropy, especially for the first barrier (on the order of $9k_B$, where k_B is the Boltzmann constant), or significant dynamical effects. The barriers for the reverse jump are 1.21 (1.11) and 0.71 (0.67) eV, with HSE06 (PBE), respectively. The values for the first jump are very close to the predicted migration energy for V_{Cu} in $CuInSe_2$.[39]

The structure with Cd in its final position is lower in energy than the starting one, which can be interpreted as a positive binding energy between Cd and the Cu interstitial (i.e., the copper atom occupying a pristine vacancy site of the $CuIn_5Se_8$ structure). Thus, the inclusion and diffusion of Cd promote disorder in the Cu network by creating Cu Frenkel pairs. Moreover, in spite of the binding energy that we just mentioned, the Cu atom sitting in a pristine vacancy site might dissociate from the Cd atom; then it will undergo interstitial migration mechanisms probably similar to those occurring in $CuInSe_2$, which have very low migration barriers (0.2−0.3 eV).[34] In this case we can expect significant correlation effects lowering the diffusion coefficient of Cd, which would support the view that Cd diffusion in the Cu-poor region of CIGS devices is faster than in stoichiometric CIGS.[4] However, a quantitative assessment of these correlation effects would imply the calculation of several additional energy barriers and their use in a kinetic Monte Carlo calculation.

CONCLUSIONS

In summary, using a combination of first-principles metadynamics simulations and static NEB calculations, we elucidated the diffusion mechanism of Cd in the OVC compound $CuIn_5Se_8$, which is a representative of the Cu-poor phases of $CuInSe_2$. We found that Cd diffuses through a kick-out mechanism occurring in two steps. The first, and rate-limiting step, with barriers of 1−1.2 eV, is the kick-out of Cu from its site to a constitutive V'_{Cu} vacancy of the material. The second step, with a barrier of 0.5−0.7 eV, consists of the displacement of Cd in the previously created Cu vacancy. The range of barrier energies reflects the difference between forward and backward jumps and the tendency of Cd to induce disorder in the Cu network. The corresponding free energy barriers at 850 K are much lower, 0.31 and 0.23 eV, showing the importance of dynamical effects.

AUTHOR INFORMATION

Corresponding Author

*E-mail: janos.kiss@cpfs.mpg.de. Phone: +49-(0)351-4646-2238.

Notes

The authors declare no competing financial interest.

ACKNOWLEDGMENTS

This work was funded by the German Bundesministerium für Umwelt, Naturschutz und Reaktorsicherheit (Project comCIGS I (No. 0327665A) and comCIGS II (No. 0325448C)). Our gratitude goes also to the Jülich Supercomputing Centre (Project HMZ22), for supercomputing support, and to the IBM, for the Shared University Research Grant. J.K. gratefully acknowledges partial financial support from the Center for Complex Matter (COMATT) at the Universität Mainz. G.R. gratefully acknowledges the Advanced Materials CEA-DEN program (MATAV) for supporting part of his stay at the University of Mainz. Markus Schmidt (IBM Mainz) is gratefully acknowledged for useful discussions.

REFERENCES

(1) Green, M. A.; Emery, K.; Hishikawa, Y.; Warta, W. Solar Cell Efficiency Tables (version 33). *Prog. Photovoltaics* **2009**, *17*, 85−94.

(2) Kaneshiro, J.; Gaillard, N.; Rocheleau, R.; Miller, E. Advances in Copper-chalcopyrite Thin Films for Solar Energy Conversion. *Sol. Energy Mater. Sol. Cells* **2009**, *94*, 12−16.
(3) Nakada, T. Nano-structural Investigations on Cd-doping Into Cu(In,Ga)Se2 Thin Films by Chemical Bath Deposition Process. *Thin Solid Films* **2000**, *361*−*362*, 346−352.
(4) Hiepko, K.; Bastek, J.; Schlesiger, R.; Schmitz, G.; Wuerz, R.; Stolwijk, N. A. Diffusion and Incorporation of Cd in Solar-grade Cu(In,Ga)Se_2 Layers. *Appl. Phys. Lett.* **2011**, *99*, 234101−1−3.
(5) Repins, I.; Contreras, M. A.; Egaas, B.; DeHart, C.; Scharf, J.; Perkins, C. L.; To, B.; Noufi, R. 19.9%-efficient ZnO/CdS/$CuInGaSe_2$ Solar Cell With 81.2% Fill Factor. *Prog. Photovoltaics* **2008**, *16*, 235−239.
(6) Rau, U.; Schock, H. W. Electronic Properties of Cu(In,Ga)Se_2 Solar Cells- Recent Achievements, Current Understanding, and Future Challenges. *Appl. Phys. A: Mater. Sci. Process.* **1999**, *69*, 131−147.
(7) Hetzer, M. J.; Strzhemechny, Y. M.; Gao, M.; Contreras, M. A.; Zunger, A.; Brillson, L. J. Direct Observation of Copper Depletion and Potential Changes at Copper Indium Gallium Diselenide Grain Boundaries. *Appl. Phys. Lett.* **2005**, *86*, 162105-1−3.
(8) Mönig, H.; Fischer, C.-H.; Caballero, R.; Kaufmann, C. A.; Allsop, N.; Gorgoi, M.; Klenk, R.; Schock, H.-W.; Lehmann, S.; Lux-Steiner, M. C.; et al. Surface Cu Depletion of Cu(In,Ga)Se_2 Films: An Investigation by Hard X-ray Photoelectron Spectroscopy. *Acta Mater.* **2009**, *57*, 3645−3651.
(9) Rockett, A.; Liao, D.; Heath, J. T.; Cohen, J. D.; Strzhemechny, Y. M.; Brillsonc, L. J.; Ramanathand, K.; Shafarmane, W. N. Near-surface Defect Distributions in Cu(In,Ga)Se_2. *Thin Solid Films* **2003**, *431*, 301−306.
(10) Liao, D.; Rockett, A. Cu Depletion at the $CuInSe_2$ Surface. *Appl. Phys. Lett.* **2003**, *82*, 2829−2831.
(11) Hofmann, A.; Pettenkofer, C. The $CuInSe_2$−$CuIn_2Se_2$ Defect Compound Interface: Electronic Structure and Band Alignment. *Appl. Phys. Lett.* **2012**, *101*, 062108-1−4.
(12) Kiss, J.; Gruhn, T.; Roma, G.; Felser, C. Theoretical Study on the Structure and Energetics of Cd Insertion and Cu Depletion of CuIn5Se8. *J. Phys. Chem. C* **2013**, *117*, 10892−10900.
(13) Liao, D.; Rockett, A. Cd Doping at the CuInSe2/CdS Heterojunction. *J. Appl. Phys.* **2003**, *93*, 9380−9382.
(14) Stolwijk, N. A.; Obeidi, S.; Bastek, J.; Wuerz, R.; Eicke, A. Fe Diffusion in Polycrystalline *Cu(In,Ga)*Se_2 Layers for Thin-film Solar Cells. *Appl. Phys. Lett.* **2010**, *96*, 244101-1−3.
(15) Obeidi, S.; Würz, R.; Frankenfeld, M.; Eicke, A.; Stolwijk, N. A. Diffusion of Iron Into Solar-grade CIGS Layers From Natural and Radioactive Front-side Sources. *Thin Solid Films* **2009**, *517*, 2205−2208.
(16) Bastek, J.; Stolwijk, N. A.; Wuerz, R.; Eicke, A.; Albert, J.; Sadewasser, S. Zinc Diffusion in Polycrystalline Cu(In,Ga)Se_2 and Single-crystal $CuInSe_2$ Layers. *Appl. Phys. Lett.* **2012**, *101*, 074105-1−3.
(17) Haarstrich, J.; Teichmann, M.; Metzner, H.; Gnauck, M.; Ronning, C.; Wesch, W.; Rissom, T.; Kaufmann, C. A.; Schock, H. W.; Scheumann, V.; et al. Buffer-free Cu(In,Ga)Se_2-solar Cells by Near-surface Ion Implantation. *Sol. Energy Mater. Sol. Cells* **2013**, *116*, 43−48.
(18) Oikkonen, L. E.; Ganchenkova, M. G.; Seitsonen, A. P.; Nieminen, R. M. Effect of Sodium Incorporation Into $CuInSe_2$ From First Principles. *J. Appl. Phys.* **2013**, *114*, 083503-1−5.
(19) Peng, H.; Xie, C.; Schoen, D. T.; McIlwrath, K.; Zhang, X. F.; Cui, Y. Ordered Vacancy Compounds and Nanotube Formation in CuInSe2-CdS Core-Shell Nanowires. *Nano Lett.* **2007**, *7*, 3734−3738.
(20) Laio, A.; Parrinello, M. Escaping Free-energy Minima. *Proc. Natl. Acad. Sci.* **2002**, *99*, 12562−12566.
(21) Iannuzzi, M.; Laio, A.; Parrinello, M. Efficient Exploration of Reactive Potential Energy Surfaces Using Car-Parrinello Molecular Dynamics. *Phys. Rev. Lett.* **2003**, *90*, 238302-1−4.
(22) Ludwig, C. D. R.; Gruhn, T.; Felser, C.; Windeln, J. Defect Structures in $CuInSe_2$: A Combination of Monte Carlo Simulations and Density Functional Theory. *Phys. Rev. B* **2011**, *83*, 174112-1−8.
(23) Jiang, F.; Feng, J. First Principles Calculation on Polytypes of Ordered Defect Compound $CuIn_5Se_8$. *Appl. Phys. Lett.* **2006**, *89*, 221920-1−3.
(24) Chang, C.-H.; Wei, S. H.; Johnson, J. W.; Zhang, S. B.; Leyarovska, N.; Bunker, G.; Anderson, T. J. Local Structure of $CuIn_3Se_5$: X-ray Absorption Fine Structure Study and First-principles Calculations. *Phys. Rev. B* **2003**, *68*, 054108-1−9.
(25) Zhang, S. B.; Wei, S. H.; Zunger, A.; Katayama-Yoshida, H. Defect Physics of the $CuInSe_2$ Chalcopyrite Semiconductor. *Phys. Rev. B* **1998**, *57*, 9642−9656.
(26) Zhang, S. B.; Wei, S. H.; Zunger, A. Stabilization of Ternary Compounds via Ordered Arrays of Defect Pairs. *Phys. Rev. Lett.* **1997**, *78*, 4059−4062.
(27) Hutter et al., *J. CPMD*, V3.15. IBM Corp 1990−2008, MPI für Festkörperforschung Stuttgart 1997−2001, see: http://www.cpmd.org.
(28) Perdew, J. P.; Burke, K.; Ernzerhof, M. Generalized Gradient Approximation Made Simple. *Phys. Rev. Lett.* **1996**, *77*, 3865−3868.
(29) Vanderbilt, D. Soft Self-consistent Pseudopotentials in a Generalized Eigenvalue Formalism. *Phys. Rev. B* **1990**, *41*, 7892−7895.
(30) Heyd, J.; Scuseria, G. E.; Ernzerhof, M. Hybrid Functionals Based on a Screened Coulomb Potential. *J. Chem. Phys.* **2003**, *118*, 8207−8215.
(31) Heyd, J.; Scuseria, G. E.; Ernzerhof, M. Erratum: "Hybrid Functionals Based on a Screened Coulomb Potential" [J. Chem. Phys. 118, 8207 (2003)]. *J. Chem. Phys.* **2006**, *124*, 219906.
(32) Kresse, G.; Furthmüller, J. Efficient Iterative Schemes for *Ab initio* Total-energy Calculations Using a Plane-wave Basis set. *Phys. Rev. B* **1996**, *54*, 11169−11186.
(33) Martyna, G. J.; Klein, M. L.; Tuckerman, M. Nosé-Hoover Chains: The Canonical Ensemble Via Continuous Dynamics. *J. Chem. Phys.* **1992**, *97*, 2635−2643.
(34) Pohl, J.; Klein, A.; Albe, K. Role of Copper Interstitials in $CuInSe_2$: First-principles Calculations. *Phys. Rev. B* **2011**, *84*, 121201-1−4.
(35) Ensing, B.; Laio, A.; Parrinello, M.; Klein, M. L. A Recipe for the Computation of the Free Energy Barrier and the Lowest Free Energy Path of Concerted Reactions. *J. Phys. Chem. B* **2005**, *109*, 6676−6687.
(36) Pietrucci, F.; Gerra, G.; Andreoni, W. *CdTe* Surfaces: Characterizing Dynamical Processes With First-principles Metadynamics. *Appl. Phys. Lett.* **2010**, *97*, 141914-1−3.
(37) Oikkonen, L. E.; Ganchenkova, M. G.; Seitsonen, A. P.; Nieminen, R. M. Mass Transport in $CuInSe_2$ From First Principles. *J. Appl. Phys.* **2013**, *113*, 133510−1−5.
(38) Henkelman, G.; Uberuaga, B. P.; Jónsson, H. A Climbing Image Nudged Elastic Band Method for Finding Saddle Points and Minimum Energy Paths. *J. Chem. Phys.* **2000**, *113*, 9901−9904.
(39) Pohl, J.; Albe, K. Thermodynamics and Kinetics of the Copper Vacancy in $CuInSe_2$, $CuGaSe_2$, $CuInS_2$, and $CuGaS_2$ From Screened-exchange Hybrid Density Functional Theory. *J. Appl. Phys.* **2010**, *108*, 023509-1−5.